PHYSICAL REVIEW B **83**, 161402(R) (2011)

# Electron-phonon interactions in bilayer graphene

K. M. Borysenko,[1] J. T. Mullen,[2] X. Li,[1] Y. G. Semenov,[1] J. M. Zavada,[1] M. Buongiorno Nardelli,[2,3] and K. W. Kim[1,*]

[1]*Department of Electrical and Computer Engineering, North Carolina State University, Raleigh, North Carolina 27695-7911, USA*

[2]*Department of Physics, North Carolina State University, Raleigh, North Carolina 27695-8202, USA*

[3]*CSMD, Oak Ridge National Laboratory, Oak Ridge, Tennessee 37831, USA*

(Received 21 March 2011; published 13 April 2011)

Using calculations from first principles, we demonstrate that *intrinsic* carrier-phonon scattering in bilayer graphene is dominated by low-energy acoustic (and acousticlike) phonon modes in a framework that bears more resemblance to bulk graphite than to monolayer graphene. The total scattering rate at low to moderate electron energies can be described by a simple two-phonon model in the deformation potential approximation with effective constants $D_{ac} \approx 15$ eV and $D_{op} \approx 2.8 \times 10^8$ eV/cm for acoustic and optical phonons, respectively. With much enhanced acoustic phonon scattering, the mobility of intrinsic bilayer graphene is estimated to be significantly smaller than that of the monolayer.

DOI: 10.1103/PhysRevB.83.161402 PACS number(s): 72.80.Vp, 63.22.Rc, 71.15.Mb, 71.38.−k

Graphene, a two-dimensional sheet of carbon atoms in a honeycomb lattice, has received wide attention due to its unique properties.[1] In addition to the significant interest in fundamental physics, which stems in part from the relativisticlike behavior of charge carriers, this material is considered very promising in many applications. The possibility of manipulating the band gap in a bilayer form[2] offers an additional control for nonlinear functionality.

While there has been a large number of reports (both experimental and theoretical) on graphene and its derivatives,[3–6] most of the studies on electron transport properties have concentrated on monolayer graphene (MLG). Among the properties requiring further investigation in bilayer graphene (BLG), intrinsic carrier-phonon scattering is one of the most crucial as it determines the ultimate limitations of any electronic device. Due to the nonpolar nature of the material, the deformation potential approximation is commonly used. However, the deformation potential constant that quantifies the strength of electron-phonon coupling must be determined outside the developed formalism in the form of an empirical fitting parameter. The experimental results lie in a broad range (e.g., $D = 10$–$50$ eV),[4–6] and further improvement of accuracy is essential for reliable analysis of transport characteristics. *Ab initio* numerical methods such as those based on density functional theory provide an alternative approach in addressing this problem as demonstrated successfully in MLG.[7,8]

In this work, we report a first-principles study of electron-phonon interaction in BLG with *AB* (Bernal) stacking. The phonon spectra and electron-phonon coupling matrix elements are calculated in the entire first Brillouin zone (FBZ) for all phonon branches based on density functional perturbation theory (DFPT).[9] The corresponding *intrinsic* scattering rates are obtained for electrons in the two lowest conduction bands by considering both intra- and interband transitions. The calculation results clearly illustrate qualitative differences from MLG, indicating significant discrepancies in transport properties. In particular, the apparent dominance of acoustic (and acousticlike) branches, together with negligibly small contributions of optical modes in a wide energy range, reveal more resemblance to bulk graphite and conventional semiconductors such as silicon. We show that the nonzero density of states near the Dirac points in BLG substantially enhances the scattering rates, which leads to a reduced electron mobility, if compared to MLG.

Figure 1 shows the calculated phonon dispersion $\omega_{\mathbf{q}}^{\nu}$ along the $\Gamma$-$K$ direction. Since there are four carbon atoms in the unit cell, BLG has 12 phonon branches. But only six lines are distinguishable across the FBZ as each of them is doubly degenerate due to the weak van der Waals coupling between the two carbon layers. The only exception, when the splitting has an appreciable magnitude, is the case of ZA (acoustic out-of-plane) and ZO′ ("layer breathing") modes near the FBZ center. In addition, two other branches deviate from the pure acoustic behavior with very small nonzero frequencies at the $\Gamma$ point as shown in Fig. 1(b) (denoted as TA2 and LA2). Hence, only three branches are truly acoustic (ZA,TA1,LA1), while we will use the term "antisymmetric acoustic" to refer to the three branches with acousticlike behavior (ZO′,TA2,LA2). Their polarization eigenvectors are akin to those of the acoustic modes in MLG, with the atomic displacements in the two layers having opposite phase (hence "antisymmetric"). The same terminology has been used in Raman spectroscopy studies.[10]

The electron spectrum $E_{\mathbf{k}}^{i}$ of BLG has two close conduction bands ($\pi_1^*$ and $\pi_2^*$); the energy gap between the bottoms of the $\pi_1^*$ (the first and lowest) and $\pi_2^*$ (the second) bands is found to be in the range 0.35–0.4 eV.[10–12] Accurate estimate of intrinsic electron scattering in BLG requires taking into account all four possible scattering scenarios: intraband ($\pi_1^* \rightarrow \pi_1^*$, $\pi_2^* \rightarrow \pi_2^*$), and interband ($\pi_1^* \rightleftarrows \pi_2^*$). Correspondingly, we calculate four sets of matrix elements $|g_{\mathbf{k}+\mathbf{q},\mathbf{k}}^{(i,j)\nu}|$ that represent the probability of electron transition from the state $(i,\mathbf{k})$ to $(j,\mathbf{k}+\mathbf{q})$, where $i$ and $j$ are the initial and final energy bands, respectively. The matrix elements are calculated only for wave vectors $\mathbf{q}$ in the irreducible Brillouin zone; the rest of the FBZ can be restored by applying the symmetry operations to vectors $\mathbf{q}$ and $\mathbf{k}$ simultaneously. The result of this calculation for *intraband scattering* ($\pi_1^* \rightarrow \pi_1^*$) of the electron at the bottom of the conduction band, e.g., $\mathbf{k} = \mathbf{K} = [2/3,0](2\pi/a)$, is shown in Fig. 2. It is not surprising that MLG-like phonon modes (ZA,TA1,LA1,ZO1,TO1,LO1) and their BLG counterparts in the doublets (ZO′,TA2,LA2,ZO2,TO2,LO2) have very similar electron-phonon matrix elements throughout

 

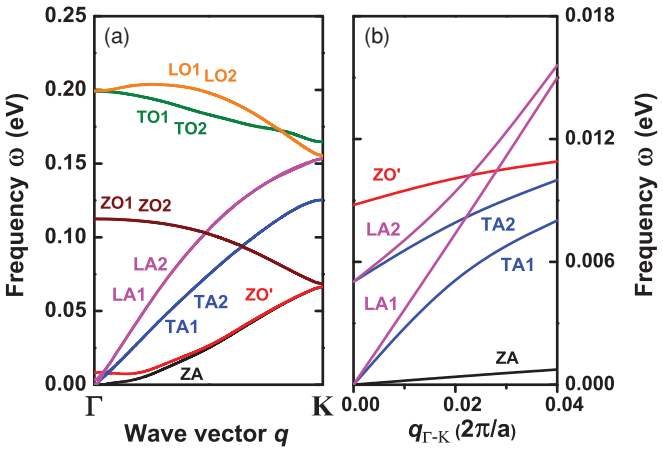


FIG. 1. (Color online) (a) Phonon spectrum of BLG along the Γ-$K$ direction. The weak interlayer coupling results in effective double degeneracy of 12 branches in BLG, everywhere in the FBZ except near the Γ point. (b) Magnified view of first six branches near the Γ point. All six lines are clearly separable. The largest splitting occurs between two out-of-plane branches: ZA and ZO′ ("breathing" mode).

the FBZ. This similarity can be explained by the relatively weak interlayer coupling in BLG, while the subtle differences between symmetric and antisymmetric modes stem from the fact that the coupling energy is finite. Strong electron

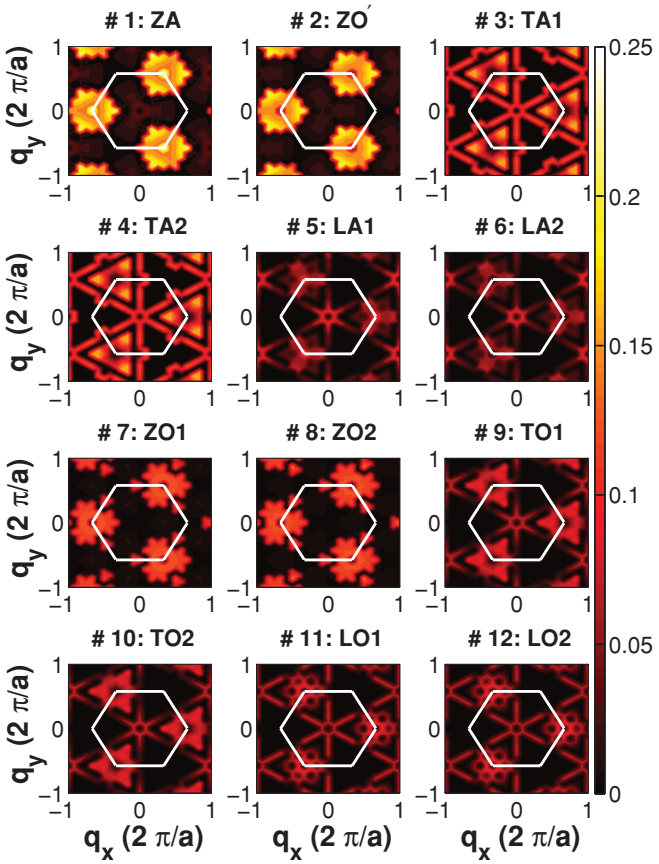


FIG. 2. (Color online) Intraband ($\pi_1^*$) matrix elements $|g^{(\pi_1^*,\pi_1^*)\nu}_{\mathbf{k}+\mathbf{q},\mathbf{k}}|$ (in units of eV) for $\mathbf{k} = [2/3,0](2\pi/a)$ (i.e., one of the Dirac points) as a function of phonon wave vector $\mathbf{q}$ and branch number $\nu$.

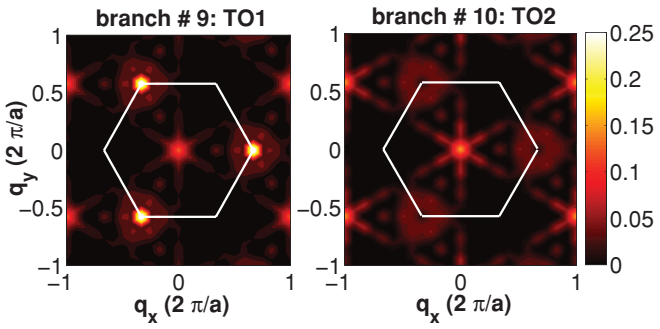


FIG. 3. (Color online) Interband matrix elements ($\pi_1^* \to \pi_2^*$) (in units of eV) for phonon branches TO1 and TO2 ($\mathbf{k} = \mathbf{K}$). The Kohn anomalies are clearly visible in the form of sharp peaks (at $\mathbf{q} = \mathbf{0}$ and $\mathbf{K}$ for TO1 and at $\mathbf{q} = \mathbf{0}$ for TO2). LO1 and LO2 also exhibit a similar peak at $\mathbf{q} = \mathbf{0}$ (not shown). The obtained result agrees with the selection rules for the electron-phonon interaction in BLG (Ref. 13).

coupling with the out-of-plane modes near the FBZ corner $\mathbf{q} = \mathbf{K}' = [1/3, 1/\sqrt{3}](2\pi/a)$ indicates that the equivalence of the two sublattices in both layers is broken as atoms $A$ and $B$ are displaced with an opposite phase. However, it is important to note that the corresponding electron transitions ($\mathbf{K} \to \Gamma$) are irrelevant to the electron-phonon scattering due to the energy conservation. As compared to MLG, the matrix elements of Fig. 2 have the same order of magnitude for the most part. One essential difference is that none of the in-plane optical phonon branches of BLG reveal Kohn anomalies at $\mathbf{q} = \mathbf{K}$ or $\mathbf{q} = \mathbf{0}$ that were prominent in MLG.[7,8]

However, further calculations show that strong peaks similar to those found in MLG do occur in the corresponding matrix elements of *interband* scattering $\pi_1^* \to \pi_2^*$. Figure 3 shows the matrix element of interband scattering $\pi_1^* \to \pi_2^*$ due to the phonons of branches 9 and 10 (TO1 and TO2). Pronounced maxima of electron-phonon coupling are clearly visible near the points of high symmetry (Fig. 3). Interestingly, the sharp peaks at $\mathbf{q} = \mathbf{K}$ are observed only in one of the TO modes (i.e., TO1), which agrees with the symmetry analysis.[13] At the same time, the Kohn anomaly at the Γ point is present in matrix elements of all four in-plane optical branches (TO1,TO2,LO1,LO2).

Based on the obtained matrix elements, the electron scattering rates are calculated using Fermi's golden rule,

$$\left(\frac{1}{\tau}\right)^{(i,j)\nu}_{\mathbf{k}} = \frac{2\pi}{\hbar}\sum_{\mathbf{q}} \left|g^{(i,j)\nu}_{\mathbf{k}+\mathbf{q},\mathbf{k}}\right|^2 \Delta^{(i,j)\nu}_{\mathbf{k},\mathbf{q}}, \qquad (1)$$

where $\Delta^{(i,j)\nu}_{\mathbf{k},\mathbf{q}} = (N^\nu_{\mathbf{q}} + \frac{1}{2} \pm \frac{1}{2})\delta(E^j_{\mathbf{k}+\mathbf{q}} - E^i_{\mathbf{k}} \pm \hbar\omega^\nu_{\mathbf{q}})$, $N^\nu_{\mathbf{q}}$ is the phonon population factor, and the plus (minus) sign corresponds to the emission (absorption) of a phonon $\omega^\nu_{\mathbf{q}}$. As we are interested in the intrinsic scattering probability that is not limited to a specific carrier distribution (and thus, the Fermi level), our formulation assumes that all final electronic states are available for transition in the bands under consideration (i.e., $\pi_1^*$ and $\pi_2^*$). The temperature dependence of the scattering rate, therefore, stems only from the the phonon occupation number. Preliminary estimates confirm that the scattering rate, as a function of the initial electron state $\mathbf{k}$ in the vicinity of the Dirac point $K$ (or $K'$), is isotropic at low energies.

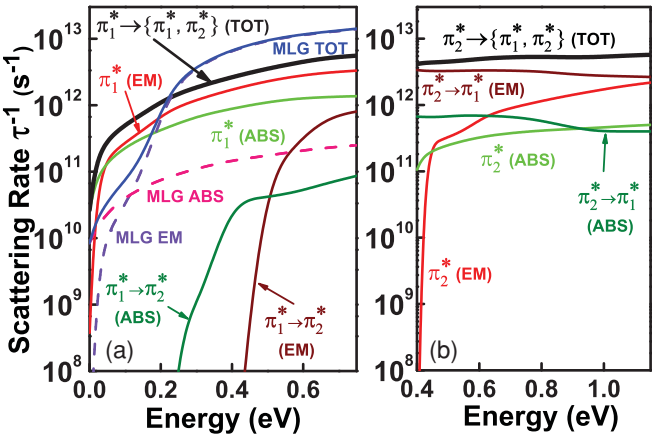


FIG. 4. (Color online) Electron-phonon scattering rates in BLG at $T = 300$ K as a function of electron energy. The initial electron state is in the (a) $\pi_1^*$ and (b) $\pi_2^*$ conduction bands, respectively. Both intra- ($\pi_i^*$) and interband ($\pi_i^* \rightarrow \pi_j^*$) transitions are considered. The $\pi_1^*$-$\pi_2^*$ band offset is 0.4 eV. ABS (EM) stands for phonon absorption (emission). TOT represents the sum of all possible interactions. In (a), the corresponding results for MLG are also plotted for comparison (Ref. 8). The reference for energy (zero) is set at the bottom of the $\pi_1^*$ band.

Accordingly, we only consider the $K$-$\Gamma$ direction in the $\mathbf{k}$ space representing $\tau^{-1}$ as a function of electron energy.

In the integration over the FBZ, an analytical expression from the tight-binding approximation is used to describe the BLG electron energy spectra in the FBZ,[2] instead of the discrete dispersion data obtained from the first-principles calculation: $E^i_{\mathbf{k}} = \sqrt{\epsilon_{\mathbf{k}}^2 + \frac{\gamma_1^2}{2} + (-1)^i[\frac{\gamma_1^4}{4} + (\gamma_1\epsilon_{\mathbf{k}})^2]^{1/2}}$, where $\epsilon_{\mathbf{k}}$ is the electron energy dispersion of MLG (as given in Ref. 2) and $i = 1,2$ for $\pi_1^*$ and $\pi_2^*$, respectively. The largest interlayer hopping integral $\gamma_1$ determines the separation between the $\pi_1^*$ and $\pi_2^*$ bands. We adopt $\gamma_1 = 0.4$ eV following recent resonant Raman studies.[11,12] Parabolic in the close vicinity of $\mathbf{k} = \mathbf{K}$ and quasilinear in a wide range beyond that, this description appears sufficient in most calculations, providing a good match to *ab initio* results at relevant electron energies.

Figure 4 shows the total scattering rates associated with all four possible scenarios involving two conduction bands. For comparison, the corresponding results of MLG from Ref. 8 are also plotted in the left panel, where initial electron states are assumed to be in the lowest conduction band. The qualitative difference between the two cases is apparent even from a cursory observation. For instance, the curves for BLG (particularly the total scattering rate) vary smoothly as a function of electron energy without any characteristic features of onset behavior. On the other hand, MLG experiences a rapid increase near 200 meV that is associated with the dominance of optical phonon emission.[8] Since BLG is also shown to exhibit Kohn anomalies at high-symmetry points (see Fig. 3), one would expect a similar effect in the overall picture of electron-phonon scattering due to the strong coupling with optical phonons. However, a detailed analysis of individual phonon branches in BLG paints a very disparate picture.

In case of intraband scattering in the band $\pi_1^*$, the scattering rate due to absorption or emission of optical phonons (ZO1,ZO2,TO1,TO2,LO1,LO2) is negligibly small in a wide range of energies ($E < 0.7$ eV). This is a direct consequence of intraband scattering matrix elements that lack strong peaks near the symmetry points as discussed earlier in reference to Fig. 2. The Kohn anomalies similar to those in MLG are observed instead in the interband scattering $\pi_1^* \rightarrow \pi_2^*$ in BLG (see Fig. 3). However, the corresponding transition rates have proven to be negligibly low. This result can be understood if one compares electron dispersions in MLG ($\pi^*$) and BLG ($\pi_1^*$ and $\pi_2^*$). A simple analysis demonstrates that electron transitions $\pi_1^* \rightarrow \pi_2^*$ involving phonons $\mathbf{q} = \mathbf{0}$ and $\mathbf{q} = \mathbf{K}$ (where the anomalies occur) are prohibited by the energy and momentum conservation laws. In other words, the contour of integration from Eq. (1) never crosses (or comes close to) the peaks at the points $\Gamma$ and $K$ observed in the matrix element of BLG. The estimated minimal distance between this curve (which can be approximated by a circle) and the point $\mathbf{q} = \mathbf{K}$ is $0.034(2\pi/a)$ for emission and $0.014(2\pi/a)$ for absorption. For comparison, the analogous distance in case of intervalley scattering due to TO phonons in MLG is much smaller, $\sim 10^{-7}(2\pi/a)$, which ensures its dominant role in electron scattering. The same consideration shows that the TO1 phonon with $\mathbf{q} = \mathbf{0}$ cannot influence the interband scattering in BLG. As a result, the total scattering rate in BLG, when the electron is initially in $\pi_1^*$ ($\pi_1^* \rightarrow \{\pi_1^*, \pi_2^*\}$), does not get a significant boost from optical phonons even at higher energies ($E_k \gtrsim 200$ meV) and becomes somewhat smaller than the total rate in MLG. The fact that the Kohn anomalies do not play an important role in the intrinsic scattering in BLG also justifies the adequacy of the DFPT calculation when compared to the more computationally demanding $GW$ approach.[7]

The situation is reversed at low energies as the curves of BLG in Fig. 4(a) reveal substantially stronger scattering rates than in MLG. This can be explained by the differences in the density of states as $\mathbf{k} \rightarrow \mathbf{K}$. More specifically, the density of states tends to zero linearly for the massless Dirac fermions of MLG while it is a constant in BLG, leading to a peculiar effect. In MLG, the intravalley scattering via acoustic phonons can be treated as quasielastic.[14,15] Consequently, the scattering rate is a linear function of energy that vanishes as $E_k \rightarrow 0$. In BLG, however, intravalley scattering with absorption of an acoustic phonon (LA1, TA1, or ZA) shows a different behavior. Aside from $\mathbf{q} = \mathbf{0}$, the energy and momentum conservation in the electron scattering allows an additional solution—a circle with radius $|\mathbf{q}| = q_{c1} = v_s\gamma_1/\hbar v_F^2$, where $v_s$ is the sound velocity. In the case of antisymmetric acoustic modes (LA2, TA2, or ZO′), an equivalent solution exists—a circle of radius $q_{c2} = \sqrt{\gamma_1\omega_\Gamma/\hbar v_F^2}$, where $\omega_\Gamma$ is the nonzero frequency of an antisymmetric acoustic mode at the $\Gamma$ point. This leads to a nonzero absorption rate even at zero electron energy. Note that a similar analysis also holds for phonon emission if electron transition to the valence band ($\pi_1$) is allowed. The impact of processes involving the $\pi_1$ band is limited only to the initial states at the bottom of $\pi_1^*$ ($E_k \ll k_BT$) and, as mentioned earlier, not included in the current calculation.

For practical application, it would be convenient to approximate the *ab initio* results for electron-phonon coupling by a simple analytical model. The deformation potential

approximation can be used to describe interaction with acoustic phonons in BLG:[6]

$$\left|g_{\mathbf{k},\mathbf{k}'}^{(\pi_1^*,\pi_1^*)(ac)}\right|^2_{\mathrm{DPA}} = \frac{D_{ac}^2\hbar q}{2A\rho v_s}\left(\frac{1+\cos 2\theta_{\mathbf{k}\mathbf{k}'}}{2}\right)\delta_{\mathbf{k}',\mathbf{k}+\mathbf{q}}\,, \quad (2)$$

where $D_{ac}$ is a deformation potential constant, $A$ is the area of the sample, $\rho$ is the mass density of BLG, and $\theta_{\mathbf{k}\mathbf{k}'}$ is the scattering angle. Note that the intravalley scattering in BLG cannot be treated quasielastically due to the additional solution with $\mathbf{q} \neq \mathbf{0}$. In fact, if only the quasielastic scattering with long-wave acoustic phonons is taken into account,[14,15] Eq. (2) leads to $\tau^{-1} = \frac{D_{ac}^2 k_B T}{2\rho v_s^2 v_F^2 \hbar^3}(\frac{\gamma_1}{2}) = \text{const}$ for $k < \gamma_1/2\hbar^2 v_F^2$ (i.e., $E_k \lesssim 200$ meV), which clearly disagrees with our calculation (see Fig. 4). Once inelastic processes are included, an excellent match to the first-principles results can be achieved with a choice of $D_{ac} \approx 15$ eV when a single branch "effectively" accounts for the contributions of all six acoustic (including antisymmetric) phonons.[16] This is much closer to the value obtained for graphite ($D_{ac} \approx 16$ eV)[17] than that for MLG ($D_{ac} \approx 4.5 - 5$ eV).[8] The scattering rates in BLG and graphite[18] turn out to be quite similar as well. The dominant intrinsic scattering mechanism in both graphite and BLG is intravalley transitions due to absorption and emission of acoustic phonons, while the contribution of the optical phonons is of secondary importance. In particular, an estimated value $D_{op} \approx 2.8 \times 10^8$ eV/cm is obtained for optical phonons in BLG using a simple model $|g_{\mathbf{k},\mathbf{k}+\mathbf{q}}^{(\pi_1^*,\pi_2^*)(op)}|^2 \simeq \frac{D_{op}^2\hbar}{2A\rho\omega_{\mathbf{q}}}$;[16] this is almost one order of magnitude smaller than in MLG.[8] With substantially enhanced acoustic phonon scattering at low energies (by nearly an order of magnitude), the intrinsic mobility of BLG estimated with a full-band Monte Carlo simulation is $\mu \approx 1.7 \times 10^5$ cm$^2$/V s (at very low or zero electron densities), which is much smaller than the corresponding quantity in MLG ($\approx 9.5 \times 10^5$ cm$^2$/V s).[8] The saturation velocity is also reduced by more than a factor of 2: $v_{\mathrm{sat}} \approx 1.8 \times 10^7$ cm/s (BLG) vs $4.2 \times 10^7$ cm/s (MLG). These values provide ideal upper bounds to experimental data that are frequently affected by individual sample conditions.

This work was supported, in part, by the DARPA/HRL CERA, ARL, and SRC/FCRP FENA programs. M.B.N. wishes to acknowledge partial support from the Office of Basic Energy Sciences, US DOE at Oak Ridge National Lab under Contract No. DE-AC05-00OR22725 with UT-Battelle, LLC. J.M.Z. acknowledges support from NSF under the IR/D program.

*kwk@ncsu.edu

[1] A. H. Castro Neto, F. Guinea, N. M. R. Peres, K. S. Novoselov, and A. K. Geim, Rev. Mod. Phys. **81**, 109 (2009).

[2] E. V. Castro, K. S. Novoselov, S. V. Morozov, N. M. R. Peres, J. M. B. Lopes dos Santos, J. Nilsson, F. Guinea, A. K. Geim, and A. H. Castro Neto, J. Phys.: Condens. Matter **22**, 175503 (2010).

[3] J.-H. Chen, C. Jang, M. Ishigami, S. Xiao, E. D. Williams, and M. S. Fuhrer, Solid State Commun. **149**, 1080 (2009).

[4] E. H. Hwang and S. Das Sarma, Phys. Rev. B **75**, 205418 (2007).

[5] E. H. Hwang and S. Das Sarma, Phys. Rev. Lett. **101**, 156802 (2008).

[6] J. K. Viljas and T. T. Heikkilä, Phys. Rev. B **81**, 245404 (2010).

[7] M. Lazzeri, C. Attaccalite, L. Wirtz, and F. Mauri, Phys. Rev. B **78**, 081406 (2008).

[8] K. M. Borysenko, J. T. Mullen, E. A. Barry, S. Paul, Y. G. Semenov, J. M. Zavada, M. B. Nardelli, and K. W. Kim, Phys. Rev. B **81**, 121412(R) (2010).

[9] S. Baroni, S. de Gironcoli, and A. Dal Corso, Rev. Mod. Phys. **73**, 515 (2001).

[10] D. L. Mafra, L. M. Malard, S. K. Doorn, H. Htoon, J. Nilsson, A. H. Castro Neto, and M. A. Pimenta, Phys. Rev. B **80**, 241414 (2009).

[11] A. Das, B. Chakraborty, S. Piscanec, S. Pisana, A. K. Sood, and A. C. Ferrari, Phys. Rev. B **79**, 155417 (2009).

[12] Z. Q. Li, E. A. Henriksen, Z. Jiang, Z. Hao, M. C. Martin, P. Kim, H. L. Stormer, and D. N. Basov, Phys. Rev. Lett. **102**, 037403 (2009).

[13] L. M. Malard, M. H. D. Guimarães, D. L. Mafra, M. S. C. Mazzoni, and A. Jorio, Phys. Rev. B **79**, 125426 (2009).

[14] F. T. Vasko and V. Ryzhii, Phys. Rev. B **76**, 233404 (2007).

[15] E. H. Hwang and S. Das Sarma, Phys. Rev. B **77**, 115449 (2008).

[16] The best fitting results for $(1/\tau)_{\mathrm{TOT}}$ are achieved when the antisymmetric acoustic branch TA2 and the optical branch TO2 are chosen, with the effective deformation potential constants $D_{ac} \approx 15$ eV and $D_{op} \approx 2.8 \times 10^8$ eV/cm, respectively. Six acousticlike (ZA,ZO′,TA1,TA2,LA1,LA2) and four optical (TO1,TO2,LO1,LO2) vibrational modes in BLG contribute almost equally in the respective groups (i.e., acoustic and optical) in a wide range of energies. Thus, the branches TA2 and TO2 are chosen simply to ensure the best fit, and not because of their exceptional role.

[17] K. Sugihara, Phys. Rev. B **28**, 2157 (1983).

[18] J. Jiang, R. Saito, A. Grüneis, G. Dresselhaus, and M. S. Dresselhaus, Chem. Phys. Lett. **392**, 383 (2004).